AIAA JOURNAL
Vol. 38, No. 3, March 2000

Boundary Element Analysis of Coupled Thermoelasticity with Relaxation Times in Finite Domain

Parissa Hosseini Tehrani* and Mohamad Reza Eslami†
Amirkabir University of Technology, 15914 Tehran, Iran

A boundary element method based on the Laplace technique is developed for transient coupled thermoelasticity problems with relaxation times in a two-dimensional finite domain. The dynamic thermoelastic model of Green and Lindsay (Green, A. E., and Lindsay, K. E., "Thermoelasticity," *Journal of Elasticity*, Vol. 2, No. 1, 1972, pp. 1–7) and Lord and Shulman (Lord, H. W., and Shulman, Y., "A Generalized Dynamic Theory of Thermoelasticity," *Journal of the Mechanics and Physics of Solids*, Vol. 15, 1967, pp. 299–309) are selected. The Laplace transform method is applied in the time domain, and the resulting equations in the transformed field are discretized using a boundary element method. The nodal dimensionless temperature and displacements in the transformed domain are inverted to obtain the actual physical quantities, using the numerical inversion of the Laplace transform method. The concern is with thermoelastic waves detection, propagation, and reflection in a finite domain that have not been reported on in the past. Comparison is made with other solutions, and coupling and relaxation time effects in stress, displacement, and temperature distribution are investigated. Details of the formulation and numerical implementation are presented.

Introduction

THE classical theory of thermoelasticity theory is based on the conventional heat conduction equation. The conventional heat conduction theory assumes that thermal disturbances propagate at infinite speeds. However, arguments questioning the validity of such a phenomenon appear in the literature for specialized applications involving very short transient durations, sudden high heat flux situations, and/or very low temperatures near absolute zero. The concept of the so-called hyperbolic nature involving finite speeds of thermal disturbance dates as far back as Maxwell.[1] Thermal disturbances of a hyperbolic nature have also been derived using various approaches.[2–4] Most of these approaches are based on the general notion of relaxing the heat flux in the classical Fourier heat conduction equation, thereby introducing a non-Fourier effect. There is also some contradiction to these nonclassical propositions in thermoelasticity, with arguments questioning application of the finite speeds of propagation in gases to those occurring in solid continua. Chester[5] provides some justification for that, noting that so-called second sound must exist in any solid because all solid continua exhibit phonon-type excitations. In an idealized solid, for example, the thermal energy can be transported by quantized electronic excitations, which are called free electrons, and by the quanta of lattice vibrations, which are called phonons. These quanta undergo collisions of a dissipative nature, causing a thermal resistance in the medium. A relaxation time t_0 is associated with the average communication time between these collisions for the commencement of resistive flow. Though the convergence time for the solutions of the hyperbolic model compared to that of the parabolic model is small, it may become important when extremely short times are involved. It is in such situations that the assumption of a parabolic heat conduction model may lead to inaccurate modeling of the transient thermal behavior. As a consequence, a hyperbolic heat conduction model that allows for both the transient heat conduction and a finite nature of thermal energy transport is argued to be a reasonable substitute for evaluating the propagation of thermal and thermally induced stress disturbances. Among the various propositions, the applicability of these nonclassical theories is well summarized by Ignaczak,[6] who includes the theories due to Lord and Shulman[7] and Green and Lindsay.[8] Excellent references are also available due to Chandrasekhariah[9] and to Joseph and Preziosi.[10,11]

Nayfeh[12] and Nayfeh and Nemat-Nasser[13] used the theory developed by Lord and Shulman[7] to study the effects of thermal coupling on both plane harmonic thermoelastic waves in unbounded media and Rayliegh surface waves propagating along the free surface of a half-space. Puri,[14] using the same theory, obtained exact solutions to the frequency equations and calculated exact values for the real and imaginary parts of the wave number. Agarwal[15] used Green and Lindsay's[8] theory to determine phase velocity, specific loss, attenuation coefficient, and amplitude ratio behavior for quasi-elastic and quasi-thermal modes by directly solving the frequency equations. Hosseini Tehrani and Eslami[16] showed the coupling effects in natural frequencies, temperature distribution, and resonance amplitudes in a time harmonic problem by using a boundary element method (BEM).

Prevost and Tao[17] demonstrated an implicit–explicit formulation adapted from a variation of the Newmark structural dynamic algorithm to solve a dynamic thermoelasticity problem based on the nonclassical model. This approach combines the algorithmic advantages of the explicit and the implicit methods into a single time integration procedure. Tamma and Railkar[18] demonstrated, via tailored hybrid transfinite element formulations, the evaluation of a particular uncoupled class of non-Fourier stress wave disturbances. Their results showed the presence of significant thermal stresses due to non-Fourier effects when the speeds of thermal waves and stress waves are equal under certain loading situations. For the case of unequal speeds of propagation, the relative magnitudes (Fourier vs non-Fourier) were shown to be almost comparable. Tamma[19] and Tamma and Namburu[20] studied various dynamic thermoelasticity problems of the nonclassical type including effective approaches for stabilizing oscillatory solution behavior. Chen and Dargush[21] used a BEM for transient and dynamic problems in generalized thermoelasticity in a half-space by using a Laplace transform and an infinite space fundamental solution. Chen and Lin[22] used a Laplace transform and control volume method to study the transient coupled thermoelastic problem with relaxation times (Green and Lindsay model[8]) in a half-space, and they found that the steep jumps occurring in the wave propagations of temperature, axial displacement, and axial stress depend on the values of the coupling coefficients and relaxation times. Chen and Lin[22] also showed two waves propagating with different but finite speeds for problems with use of Green and Lindsay's[8] dynamic thermoelastic model. Eslami and Hosseini Tehrani[23] considered boundary element formulation for conventional coupled thermoelasticity in a two-dimensional finite

Received 22 May 1998; revision received 23 June 1999; accepted for publication 22 July 1999.

*Graduate Student, Mechanical Engineering Department.
†Professor, Mechanical Engineering Department. Associate Fellow AIAA.

domain and investigated the coupling effect in temperature, displacement, and stress distribution.

With the advent of laser technology, in which high-heat-flux conditions are encountered, its use for extremely short durations has found many applications. Some typical applications include the annealing of semiconductors, surface heating, and melting of metals. Other applications include explosive bonding and melting where high local heat fluxes are involved, for nucleate boiling, etc. The basic nature of thermal energy transport immediately after the application of the pulse and the resulting sustained temperature at the surface of the medium have been some topics of interest in such situations.

In this paper, a Laplace transform BEM is developed for the dynamic problem in coupled thermoelasticity with relaxation times involving a finite two-dimensional domain. The boundary element formulation is presented, and a single heat excitation is used to drive the boundary element formulations. Aspects of the numerical implementation are discussed. It is seen through various illustrative problems that the present method has good accuracy and efficiency in predicting the wave propagations of temperature, displacement, and stress. Note that the distributions of temperature, displacement, and stress show jumps at their wave fronts. Thermomechanical waves propagation and reflection in a finite domain are investigated, and the influences of coupling parameter and relaxation times on thermoelastic waves are also investigated.

Throughout this paper, the summation convention on repeated indices is used. A dot indicates time differentiation, and the subscript i after a comma is partial differentiation with respect to x_i ($i = 1, 2$).

Governing Equations

A homogeneous isotropic thermoelastic solid is considered. In the absence of body forces and heat flux, the governing equations for the dynamic coupled generalized thermoelasticity in the time domain are

$$(\lambda + \mu)u_{j,ij} + \mu u_{i,jj} - \gamma T_0(T_{,i} + t_1\dot{T}_{,i}) - \rho\ddot{u}_i = 0 \tag{1}$$

$$kT_{,jj} - \rho c_e\dot{T} - \rho c_e(t_0 + t_2)\ddot{T} - \gamma(t_0\ddot{u}_{i,i} + \dot{u}_{i,i}) = 0 \tag{2}$$

where λ, μ, u_i, ρ, T, T_0, k, γ, c_e, t_0, t_1, and t_2 are Lame's constant, the two components of the displacement vector, density, absolute temperature, reference temperature, conductivity, stress–temperature modulus, specific heat, relaxation time proposed by Lord and Shulman[7] (LS), and the two relaxation times proposed by Green and Lindsay[8] (GL), respectively. When t_0, t_1, and t_2 vanish, Eqs. (1) and (2) reduce to classical coupled theory. In LS theory, $t_1 = t_2 = 0$, and Fourier's law of heat conduction is modified by introducing the relaxation time t_0. In GL theory, $t_0 = 0$, and both the Duhamel–Neuman relations and entropy density function are modified by introducing two relaxation times t_1 and t_2 (Ref. 17). It is convenient to introduce the usual dimensionless variables as follows:

$$\hat{x} = \frac{x}{\alpha}, \qquad \hat{t} = \frac{tC_1}{\alpha}, \qquad \hat{t}_0 = \frac{t_0C_1}{\alpha}, \qquad \hat{t}_1 = \frac{t_1C_1}{\alpha}$$

$$\hat{t}_2 = \frac{t_2C_1}{\alpha}, \qquad \hat{\sigma}_{ij} = \frac{\sigma_{ij}}{\gamma T_0}, \qquad \hat{u}_i = \frac{(\lambda + 2\mu)u_i}{\alpha \cdot \gamma \cdot T_0}$$

$$\hat{T} = \frac{T - T_0}{T_0} \tag{3}$$

where $\alpha = k/\rho c_e C_1$ is the dimensionless unit length and $C_1 = \sqrt{(\lambda + 2\mu)/\rho}$ is the velocity of the longitudinal wave. Equations (1) and (2) take the form (dropping the caret for convenience)

$$[\mu/(\lambda + 2\mu)]u_{i,jj} + [(\lambda + \mu)/(\lambda + 2\mu)]u_{j,ij} - (T_{,i} + t_1\dot{T}_i) - \ddot{u}_i = 0 \tag{4}$$

$$T_{,jj} - \dot{T} - (t_0 + t_2)\ddot{T} - \frac{T_0\gamma^2}{\rho c_e(\lambda + 2\mu)}(\dot{u}_{j,j} + t_0\ddot{u}_{j,j}) = 0 \tag{5}$$

At these dimensionless equations, the stress wave speed is one, and the speed of the temperature wave may be computed as[17]

$$C_t = \sqrt{1/(t_0 + t_2)} \tag{6}$$

Transferring Eqs. (4) and (5) to the Laplace domain yields

$$[\mu/(\lambda + 2\mu)]u_{i,jj} + [(\lambda + \mu)/(\lambda + 2\mu)]u_{j,ij} - (T_{,i} + t_1T_{,i}) - s^2u_i = 0 \tag{7}$$

$$T_{,ii} - sT - (t_0 + t_2)s^2T - \frac{T_0\gamma^2}{\rho c_e(\lambda + 2\mu)}(su_{j,j} + t_0s^2u_{j,j}) = 0 \tag{8}$$

Equations (7) and (8) are rewritten in matrix form as

$$L_{ij}U_j = 0 \tag{9}$$

For the two-dimensional domain, the operator L_{ij} reduces to

$$L_{ij} = \begin{bmatrix} \frac{\mu}{\lambda + 2\mu}\Delta + \frac{\lambda + \mu}{\lambda + 2\mu}D_1^2 - s^2 & \frac{\lambda + \mu}{\lambda + 2\mu}D_1D_2 & -D_1(1 + t_1s) \\ \frac{\lambda + \mu}{\lambda + 2\mu}D_1D_2 & \frac{\mu}{\lambda + 2\mu}\Delta + \frac{\lambda + \mu}{\lambda + 2\mu}D_2^2 - s^2 & -D_2(1 + t_1s) \\ -\frac{T_0\gamma^2}{\rho c_e(\lambda + 2\mu)}s(1 + t_0s)D_1 & -\frac{T_0\gamma^2}{\rho c_e(\lambda + 2\mu)}s(1 + t_0s)D_2 & \Delta - s(1 + st_0 + st_2) \end{bmatrix}$$

$$U_i = [u \quad v \quad T]$$

where $D_i = \partial/\partial x_i$ ($i = 1, 2$) and Δ denotes the Laplacian. The boundary conditions are assumed to be

$$\begin{aligned} u_i &= \hat{u}_i && \text{on} && \Gamma_u \\ \tau_i &= \sigma_{ij}n_j && \text{on} && \Gamma_\tau \\ T &= \hat{T} && \text{on} && \Gamma_T \\ q &= q_in_i && \text{on} && \Gamma_q \end{aligned} \tag{10}$$

Boundary Integral Equation

To drive the boundary integral problem, we start with the following weak formulation of the differential equation set (9) for the fundamental solution tensor V_{ik}^*:

$$\int_\Omega (L_{ij}U_j)V_{ik}^* \, d\Omega = 0 \tag{11}$$

After integrating by parts over the domain and taking a limiting procedure approaching the internal source point to the boundary point, we can obtain the following boundary integral equation:

$$C_{kj}U_k(y, s) = \int_\Gamma \tau_\alpha(x, s)V_{\alpha j}^*(x, y, s) - U_\alpha(x, s)\Sigma_{\alpha j}^*(x, y, s)\, d\Gamma(x) + \int_\Gamma T_{,n}(x, s)V_{3j,n}^*(x, y, s) - T(x, s)V_{3j,n}^*(x, y, s)\, d\Gamma(x) \tag{12}$$

where $U_\alpha = u_\alpha$ ($\alpha = 1, 2$), $U_3 = T$, and C_{kj} denotes the shape coefficient tensor. The kernel

$$\Sigma_{\alpha j}^*$$

in Eq. (12) is defined by

$$\Sigma^*_{\alpha j} = \left\{ \left(\frac{\lambda}{\lambda + 2\mu} V^*_{kj,k} + \frac{T_0 \gamma^2 (s + t_0 s^2)}{\rho C_e (\lambda + 2\mu)} V^*_{3j} \right) \delta_{\alpha\beta} + \frac{\mu}{\lambda + 2\mu} \left(V^*_{\alpha j,\beta} + V^*_{\beta j,\alpha} \right) \right\} n_\beta \tag{13}$$

Here the fundamental solution tensor V_{jk} must satisfy the differential equation

$$l_{ij} V^*_{jk} = -\delta_{ik} \delta(x - y) \tag{14}$$

where l_{ij} is the adjoint operator of L_{ij} in Eq. (9) and is given by

$$l_{ij} = \begin{bmatrix} \frac{\mu}{\lambda + 2\mu}\Delta + \frac{\lambda + \mu}{\lambda + 2\mu} D_1^2 - s^2 & \frac{\lambda + \mu}{\lambda + 2\mu} D_1 D_2 & \frac{T_0 \gamma^2}{\rho c_e (\lambda + 2\mu)} (s + t_0 s^2) D_1 \\ \frac{\lambda + \mu}{\lambda + 2\mu} D_1 D_2 & \frac{\mu}{\lambda + 2\mu}\Delta + \frac{\lambda + \mu}{\lambda + 2\mu} D_2^2 + s^2 & \frac{T_0 \gamma^2}{\rho c_e (\lambda + 2\mu)} (s + t_0 s^2) D_2 \\ D_1 (1 + t_1 s) & D_2 (1 + t_1 s) & \Delta - s(1 + t_0 s + t_2 s) \end{bmatrix}$$

Fundamental Solution

To construct the fundamental solution, we put the fundamental solution tensor V^*_{ij} of Eq. (14) in the following potential representation by using the transposed cofactor operator μ_{ij} of l_{ij} and scalar function Φ^* (Ref. 24):

$$V^*_{ij}(x, y, s) = \mu_{ij} \Phi^*(x, y, s) \tag{15}$$

After substitution of Eq. (15) into Eq. (14), we can get the following differential equations:

$$\Lambda \Phi^* = -\delta(x - y) \tag{16}$$

where

$$\Lambda = \det(l_{ij}) = [\mu/(\lambda + 2\mu)] (\Delta - h_1^2)(\Delta - h_2^2)(\Delta - h_3^2) \tag{17}$$

where the h_i^2 are

$$h_1^2 = \frac{\lambda + 2\mu}{\mu} s^2$$

$$h_2^2 + h_3^2 = s^2 + s(1 + t_0 s + t_2 s) + \frac{T_0 \gamma^2}{\rho C_e (\lambda + 2\mu)} s (1 + t_0 s + t_1 s + t_0 t_1 S^2)$$

$$h_2^2 h_3^2 = s^3 (1 + t_0 s + t_2 s) \tag{18}$$

where h_1 is the longitudinal wave velocity, h_2 the shear wave velocity, and h_3 the rotational wave velocity and where

$$\Phi = \frac{\lambda + 2\mu}{2\pi\mu} \left[\frac{K_0(h_1 r)}{(h_2^2 - h_1^2)(h_3^2 - h_1^2)} + \frac{K_0(h_2 r)}{(h_3^2 - h_2^2)(h_1^2 - h_2^2)} + \frac{K_0(h_3 r)}{(h_1^2 - h_3^2)(h_2^2 - h_3^2)} \right] \tag{19}$$

The fundamental solution tensor V^*_{ij} for the two-dimensional domain is found as follows:

$$V^*_{\alpha\beta} = \sum_{k=1}^{3} [\psi_k(r) \delta_{\alpha\beta} - \kappa_k r_{,\alpha} r_{,\beta}] \qquad (\alpha, \beta = 1, 2)$$

$$V^*_{3\alpha} = \sum_{k=1}^{3} \xi'_k(r) r_{,\alpha}, \qquad V^*_{\alpha 3} = \sum_{k=1}^{3} \xi_k(r) r_{,\alpha}, \qquad V^*_{33} = \sum_{k=1}^{3} \zeta_k(r) \tag{20}$$

where

$$\psi_k(r) = \frac{W_k}{2\pi} \left((h_k^2 - m_2)(h_k^2 - m_1) + \left(\frac{\lambda + \mu}{\mu} \right) \left(h_k^2 - m_1 - m_3 m_4 C \frac{\lambda + 2\mu}{\lambda + \mu} \right) h_k^2 \right) K_0(h_k r) + \frac{W_k (\lambda + \mu)}{2\pi\mu} \times \left(h_k^2 - m_1 - m_3 m_4 C \frac{\lambda + 2\mu}{\lambda + \mu} \right) \frac{h_k}{r} K_1(h_k r)$$

$$\kappa_k(r) = \frac{W_k (\lambda + \mu)}{2\pi\mu} \left(h_k^2 - m_1 - m_3 m_4 C \frac{\lambda + 2\mu}{\lambda + \mu} \right) K_2(h_k r)$$

$$\xi'_k(r) = \frac{W_k}{2\pi} m_4 (h_k^2 - m_2) h_k K_1(h_k r)$$

$$\xi_k(r) = \frac{W_k}{2\pi} C m_3 (h_k^2 - m_2) h_k K_1(h_k r)$$

$$\zeta_k(r) = \frac{W_k}{2\pi} (h_k^2 - m_2)(h_k^2 - s^2) K_0(h_k r) \tag{21}$$

$$r = \|x - y\|, \qquad m_1 = s(1 + t_0 s + t_2 s), \qquad m_2 = \frac{\lambda + 2\mu}{\mu} s^2$$

$$m_3 = s(1 + t_0 s), \qquad m_4 = (1 + t_1 s), \qquad C = \frac{T_0 \gamma^2}{\rho c_e (\lambda + 2\mu)}$$

$$W_i = \frac{-1}{(h_i^2 - h_j^2)(h_k^2 - h_i^2)}$$

$$(i = 1, 2, 3, \qquad j = 2, 3, 1, \qquad k = 3, 2, 1) \tag{22}$$

and $K_0(h_k r)$, $K_1(h_k r)$, and $K_2(h_k r)$ are the modified Bessel functions of the second kind and of zero, first, and second orders, respectively. To solve numerically the boundary element integral equation (12), the standard procedure is applied. When transformed numerical solutions are specified, transient solutions can be obtained by using an appropriate numerical inversion technique. In this paper, a method presented by Durbin[25] is adopted for this numerical inversion.

Numerical Examples

The following examples are considered to investigate the accuracy and efficiency of the method. To compare the two-dimensional numerical results of this paper with the analytically known solution of a half-space, a square plate subjected to heating at one edge with a step function is considered (Fig. 1). The plate is thermally isolated at the three other edges. The plate material considered is stainless steel. Results are obtained along the axis of symmetry of the plate. The boundary element solution and the analytical solution of the coupled and uncoupled thermoelasticity of a half-space are given by Chen and Dargush[21] and Sternberg and Chakravorty,[26] respectively. Both solutions are based on the Laplace transform method. Figures 2–4 show a comparison of the dimensionless temperature, axial displacement, and axial stress at dimensionless length $x = 1$ (which is the location of the elastic wave front at the nondimensional time $t = 1$). The results are plotted for the analytical solutions,[26] the boundary element solutions[21] and the present results for different coupling parameters. The case $C = 0$ corresponds to the uncoupled solution. Coupled results are presented for $C = 0.36$ and 1 to match the results of Chen and Dargush.[21] These values are unrealistically high for the material of interest. The data that are considered for comparison purposes (Figs. 2–4) are related to the solution of coupled

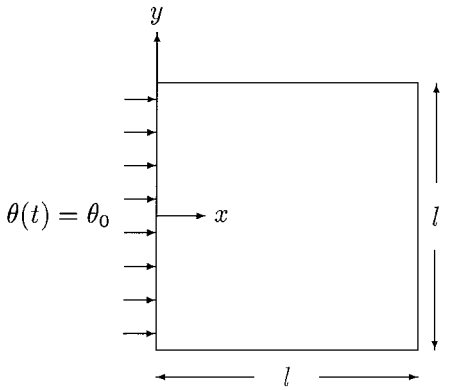

Fig. 1 Square plate subjected to thermal loading.

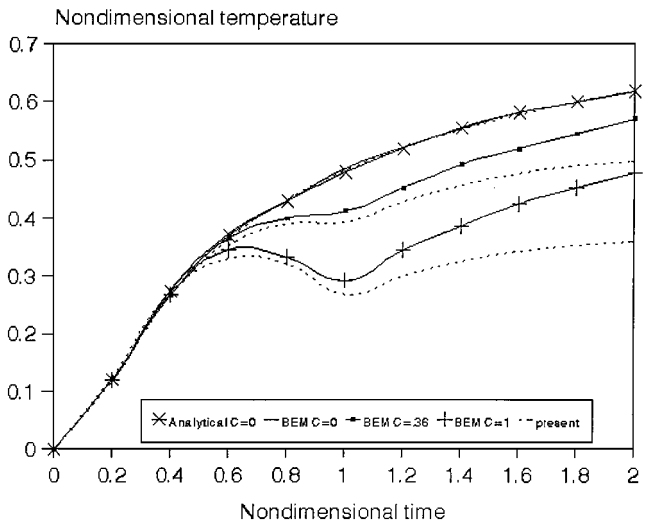

Fig. 2 Comparison of the dimensionless temperature at $x = 1$.

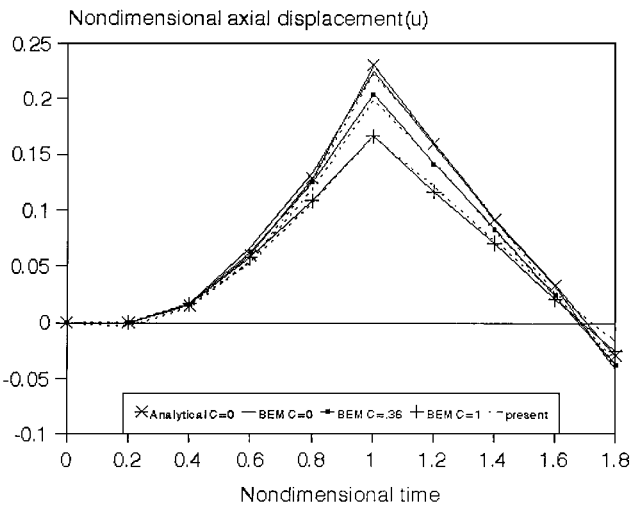

Fig. 3 Comparison of the dimensionless axial displacement at $x = 1$.

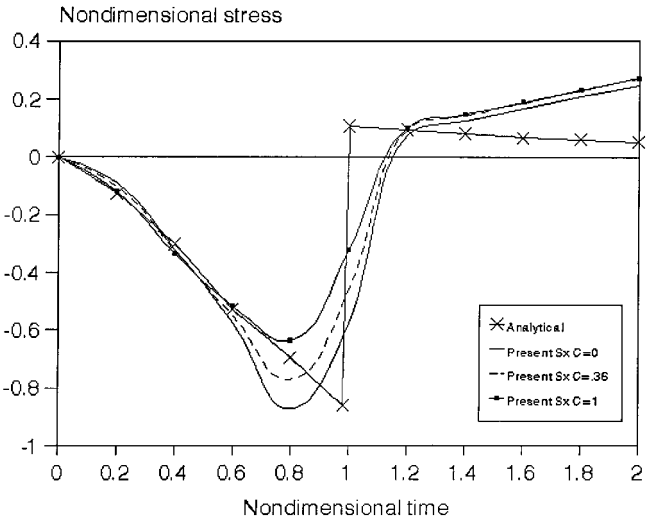

Fig. 4 Comparison of the dimensionless axial stress at $x = 1$.

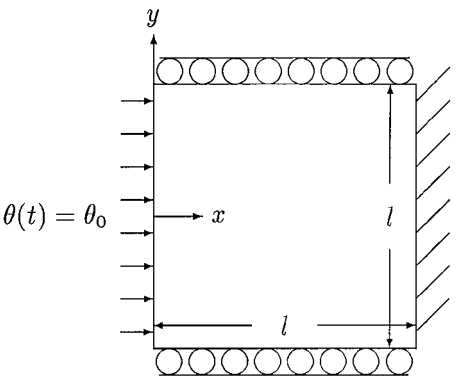

Fig. 5 Model of a layer subjected to thermal loading.

thermoelasticity in half-space. In the half-space region, the solution domain reduces to a one-dimensional problem. It is seen that the displacement and uncoupled temperature results of the present paper have good agreement with analytical and boundary element solutions for the different coupling parameters. However, the coupled temperature and stress solution of the present paper deviates from the half-space solution as time is advanced.

For the uncoupled condition, the temperature equation is solved separately for the temperature distribution and is independent of the stress field. Because the data presented in Figs. 2–4 are related to the axis of symmetry of the plate, $q_y = k(\partial T/\partial y)$ is zero and the temperature distribution is symmetric about the x axis. Consequently, the distribution of the temperature along the axis of symmetry of a two-dimensional domain coincides with that of the one-dimensional solution of the half-space. For the coupled solution, however, the influence of the stress field in the temperature distribution of a two-dimensional domain results in a lower temperature curve compared to the half-space solution. The displacement curves of the two-dimensional domain along the axis of symmetry of the domain almost coincide with those of half-space. The reason is that due to symmetry $v = 0$ along the x axis and the only nonzero displacement is u. This condition coincides with the one-dimensional half-space solution. The stress plot of the two-dimensional domain along the axis of symmetry, shown in Fig. 4, is different from that of the half-space. The main reason for the difference is the existence of nonzero ϵ_y in the two-dimensional domain. The effect of ϵ_y causes the peak of compressive stress to occur at a shorter time. The tensile stress produced by the application of thermal shock is larger in a finite domain compared to the half-space. This is shown in Fig. 4 for the range of time where the wave reflection is not yet produced.

Now consider a coated surface subjected to a laser beam. Because the effects of the coupled thermoelastic field is in general significant at a very short time in the early stages of thermal shock application, the stress field is studied in the coated domain. When the length is too long compared to thickness, as it is in the case of a coated surface, the problem can be modeled as shown in Fig. 5. To compare the results with the solutions available for the half-space, the square plate ($l = 2$ nondimensional) of Fig. 5 is considered to experience a step function heating in one side and to be isolated at the other sides. The thermoelastic wave propagation, reflection, and the effect of relaxation times are investigated along the axis of symmetry of the plate in unit dimensionless length and are compared with the

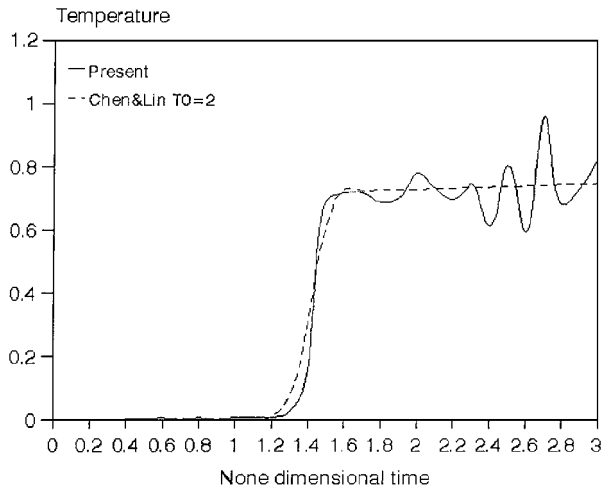

Fig. 6 Comparison of the dimensionless temperature at middle of the plate for LS theory.

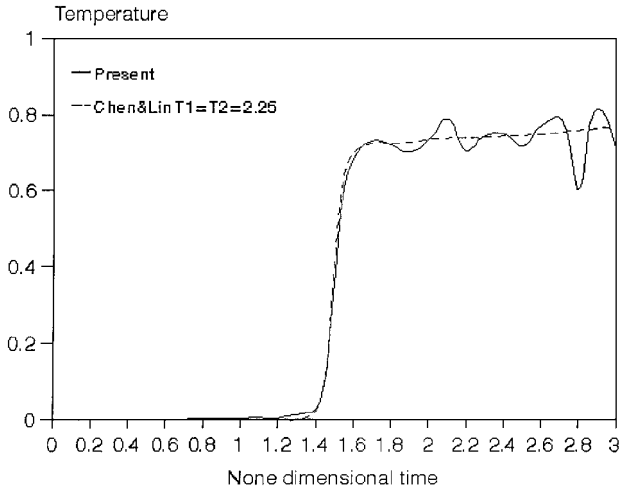

Fig. 7 Comparison of the dimensionless temperature at middle of the plate for GL theory.

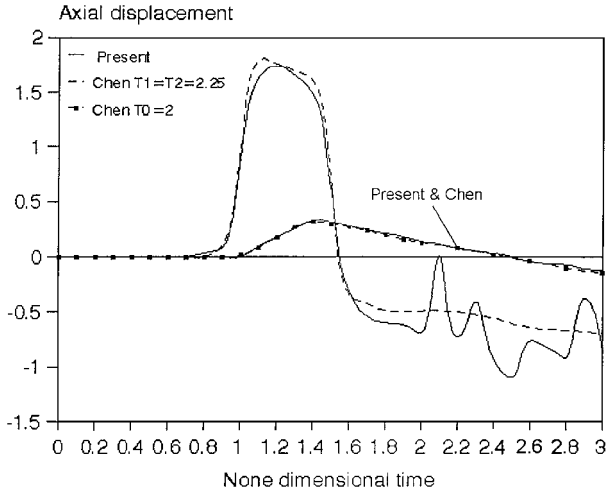

Fig. 8 Comparison of the dimensionless axial displacement at middle of the plate for LS and GL theories.

half-space results (Figs. 6–10). Then the thermal load equation at $x = 0$ is considered as (Fig. 11)

$$\theta(t) = t \exp^{-5t} \tag{23}$$

The thermoelastic waves fronts propagation with different speeds and the relaxation time effects for GL and LS theories are shown along the axis of symmetry of the plate (Figs. 12–19). These results are reported for the first time in this paper. Figures 6–8 show dimensionless temperature and displacement distribution vs dimensionless time for LS and GL theories with a zero coupling parameter. The temperature distribution shows osculation after the temperature wave front due to the temperature wave reflection from the boundaries for both the LS and GL theories in a finite domain. Axial displacement distribution in the LS model has good adaptation with the half-space result. In the GL model, the temperature variation has more effect on the displacement (t_1 effect). After temperature wave front, in GL theory, displacement distribution oscillates and deviates from the half-space result. Figures 9 and 10 show

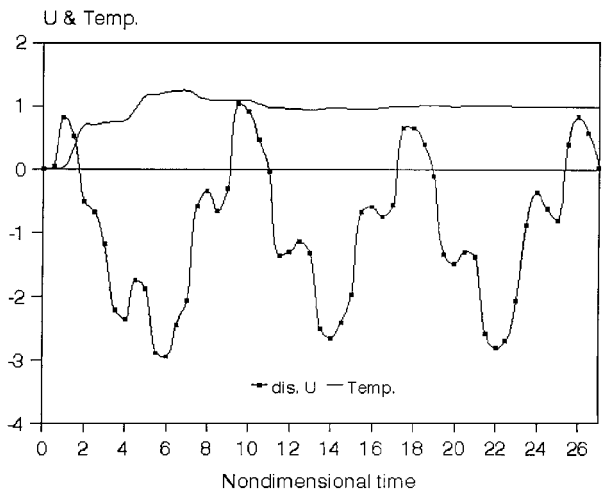

Fig. 9 Temperature and axial displacement distribution at middle of the plate for GL model ($t_1 = t_2 = 2.25$) over time.

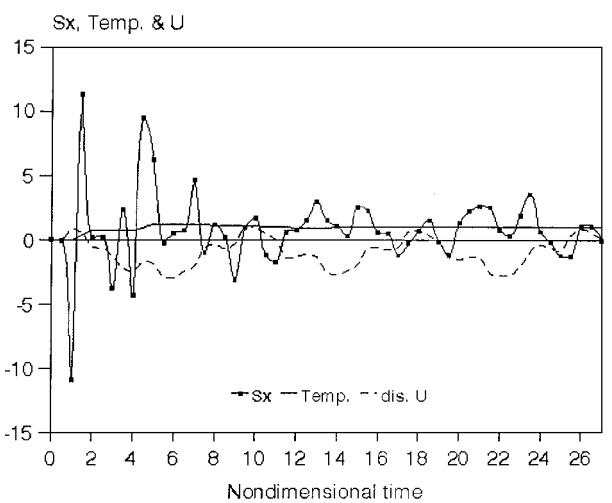

Fig. 10 Temperature, axial displacement, and stress distribution at middle of the plate for GL model ($t_1 = t_2 = 2.25$) over time.

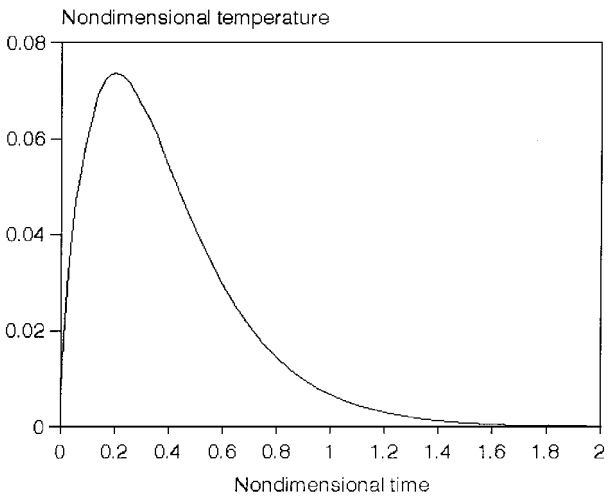

Fig. 11 Pattern of thermal loading.

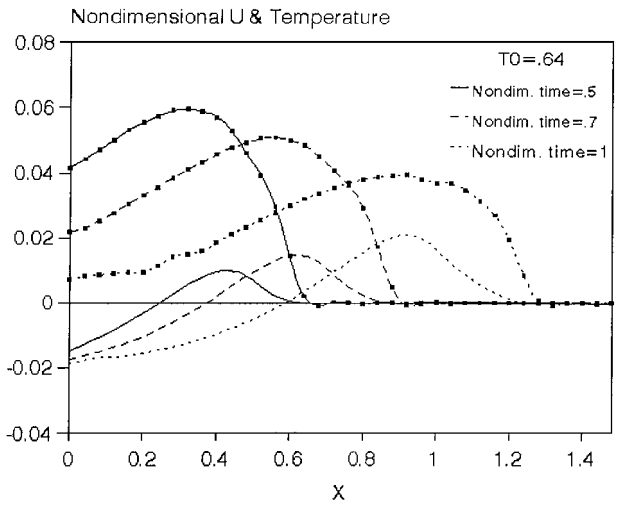

Fig. 12 Distribution of the dimensionless temperature and axial displacement along the axis of symmetry of domain shown in Fig. 5 for LS theory: $T_0 = 0.64$; symbols demonstrate temperature distribution.

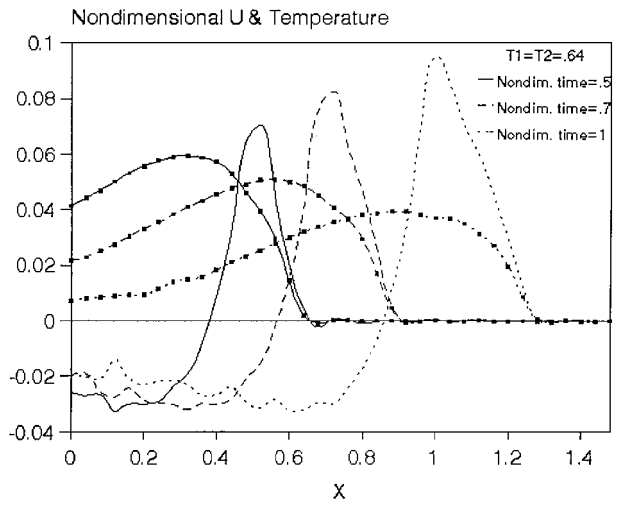

Fig. 13 Distribution of the dimensionless temperature and axial displacement along the axis of symmetry of domain shown in Fig. 5 for GL theory: $T_1 = T_2 = 0.64$; symbols demonstrate temperature distribution.

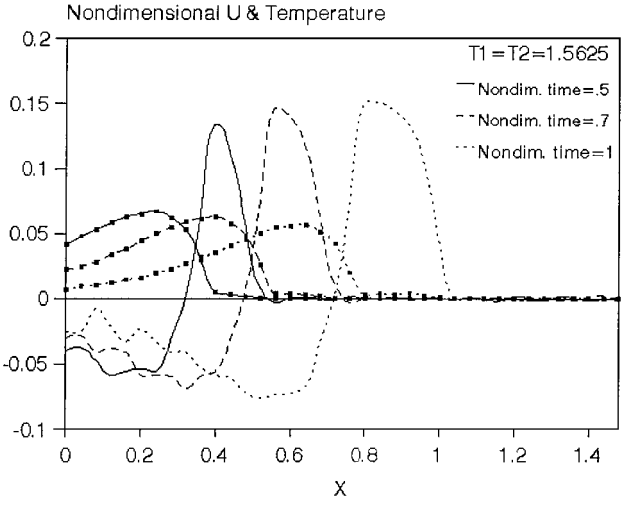

Fig. 14 Distribution of the dimensionless temperature and axial displacement along the axis of symmetry of domain shown in Fig. 5 for GL theory: $T_1 = T_2 = 1.5625$; symbols demonstrate temperature distribution.

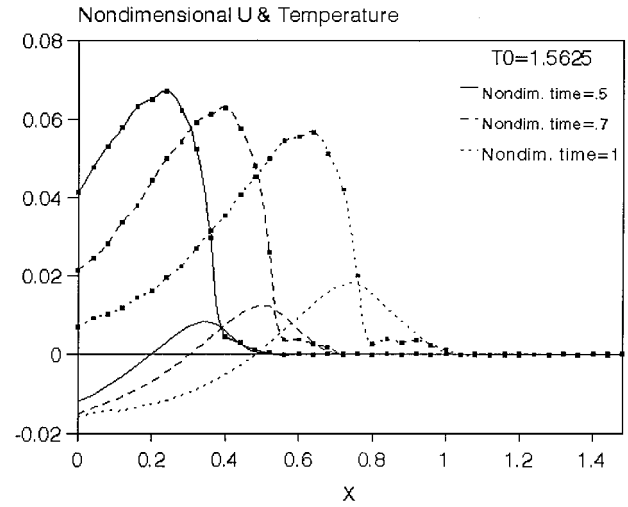

Fig. 15 Distribution of the dimensionless temperature and axial displacement along the axis of symmetry of domain shown in Fig. 5 for LS theory: $T_0 = 1.5625$; symbols demonstrate temperature distribution.

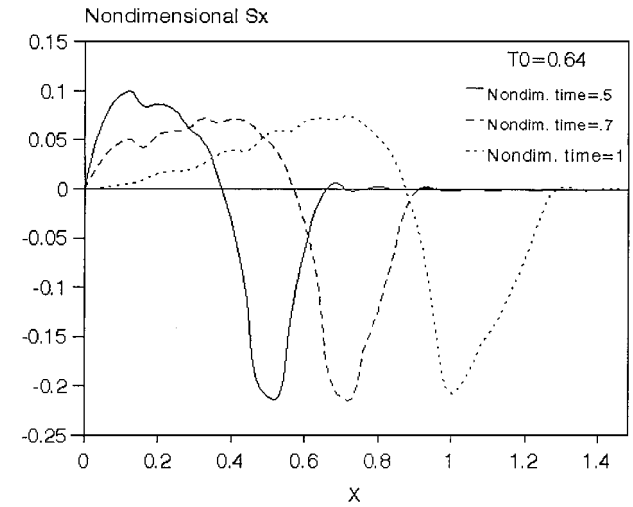

Fig. 16 Distribution of the dimensionless axial stress along the axis of symmetry of domain shown in Fig. 5 for LS theory: $T_0 = 0.64$.

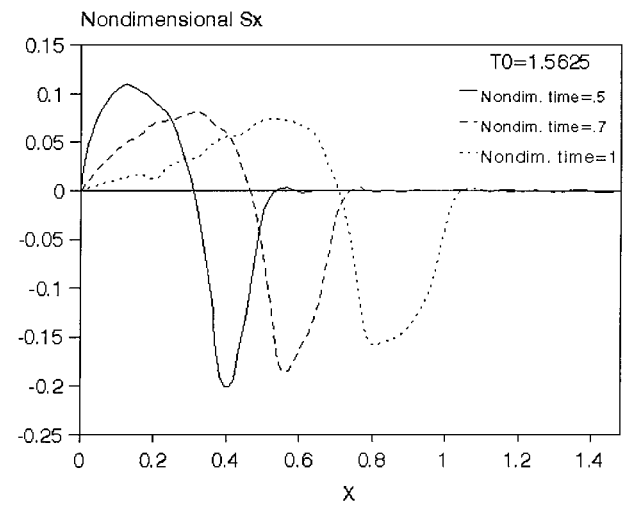

Fig. 17 Distribution of the dimensionless axial stress along the axis of symmetry of domain shown in Fig. 5 for LS theory: $T_0 = 1.5625$.

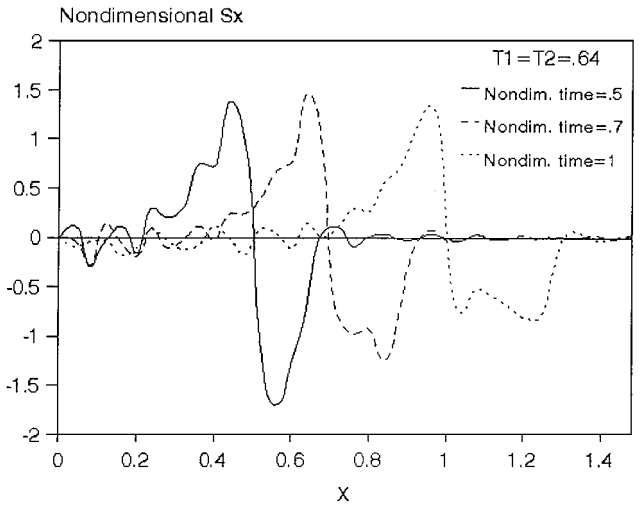

Fig. 18 Distribution of the dimensionless axial stress along the axis of symmetry of domain shown in Fig. 5 for GL theory: $T_1 = T_2 = 0.64$.

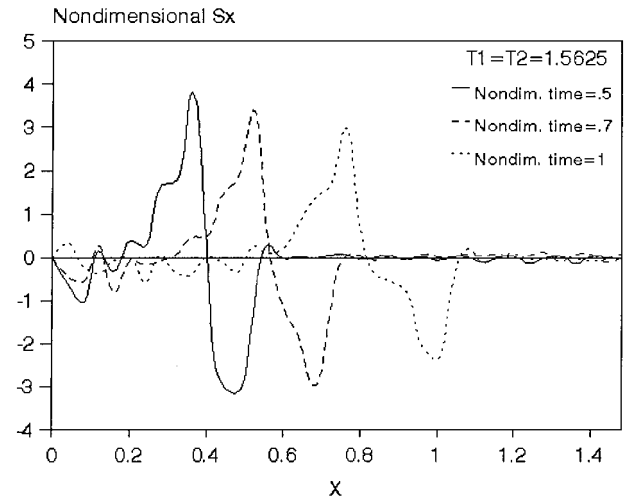

Fig. 19 Distribution of the dimensionless axial stress along the axis of symmetry of domain shown in Fig. 5 for GL theory: $T_1 = T_2 = 1.5625$.

temperature, axial displacement, and stress distribution for three first periods of vibration under step temperature loading. The temperature distribution after two jumps approaches the input temperature. The first jump demonstrates the temperature wave front, and the second jump shows how the reflected temperature wave from the front isolated surface adds to the first wave. When this augmented wave reaches the surface with fixed input temperature $\theta_0 = 1$, a negative temperature gradient is created, and finally the temperature becomes equal with input temperature. Figure 9 clearly shows the periodic pattern of displacement. Figure 10 shows, when the temperature jumps are diminished, the stress variation approach to periodic motion and the initial abrupt variations of stress are damped. Figures 12–19 show temperature, axial displacement, and stress distribution along the axis of symmetry of the domain shown in Fig. 5 under the temperature loading of Eq. (23). The coupling parameter is 0.0168. It seems that temperature distribution is nearly the same for two theories, but displacement and stress results for the GL theory, especially when the stress wave speed is faster than the thermal waves, are many times the results for the LS theory. Figures 12–19 also show that the peak values of the temperature decrease with increasing value of x. In the LS and GL theories, it is expected to have two waves propagate with different but finite speeds. The propagation speed of the elastic wave is faster than that of the thermal wave for t_0 or $t_2 > 1$. Figures 16–19 clearly show this phenomenon for the stress distribution. As the value of x is increased, the zone between the two steep jumps in the axial stress distribution grow wider. One of these jumps is located on the temperature wave front and the other on the stress wave front. These finding (Figs. 12–19) for the LS and GL theories in a finite domain were not reported in the past.

Conclusion

In the present work, a hybrid application of the Laplace transform and BEM is applied to analyze the generalized thermoelastic problems of two-dimensional finite domain and various loadings. The integral representation is derived directly from the governing differential equations in the Laplace domain. By utilizing the infinite space adjoint fundamental solution, a boundary element formulation is obtained, thus eliminating the need for volume discretization for the analysis of homogeneous media. Comparison with an available half-space solution is made, and the applicability of the method is shown.

It is found from the present study that the magnitudes of the step jumps occurring in the wave propagations of temperature, axial displacement, and axial stress depend on the values of the coupling coefficients, relaxation times, chosen theory, etc. The important conclusions of this paper are as follows.

1) Application of the Laplace transform in the time domain, instead of other marching methods, causes realistic evaluation of field variables in coupled thermoelasticity. Traditionally, the coupled thermoelasticity problems in engineering structures are evaluated by numerical methods, such as the finite element method, where time marching techniques are employed to solve the finite element equilibrium equation. Many facts are lost in these types of analyses due to the inadequate timescale increment.

2) Wave reflections are seen in the finite domain, whereas in infinite space these phenomena are not observed.

3) Two wave fronts with different and finite speed are observed in the distribution of temperature, displacement, and stress. It was shown that the elastic stress wave is faster than the thermal wave for t_0 or $t_2 > 1$.

References

[1]Maxwell, J. C., "On the Dynamical Theory of Gases," *Philosophical Transactions of the Royal Society of London*, Vol. 157, 1867, pp. 49–88.

[2]Landau, E. M., "The Theory of Superfluidity of Helium II," *Journal of Physics, USSR*, Vol. 5, 1941, pp. 71–90.

[3]Peshkov, V., "Second Sound in Helium II," *Journal of Physics, USSR*, Vol. 8, 1944, pp. 131–138.

[4]Vernotte, P., "Les Paradoxes de la theorie continue de l'equation de la chaleur," *Comptes Rendus Hebdomadaires des Seances de l'Academie des Sciences*, Vol. 246, 1958, pp. 3154, 3155.

[5]Chester, M., "Second Sound in Solids," *Physical Review*, Vol. 131, 1963, pp. 2013–2015.

[6]Ignaczak, J., "Linear Dynamic Thermoelasticity—A Survey," *Shock and Vibration Digest*, Vol. 13, 1980, pp. 3–8.

[7]Lord, H. W., and Shulman, Y., "A Generalized Dynamic Theory of Thermoelasticity," *Journal of the Mechanics and Physics of Solids*, Vol. 15, 1967, pp. 299–309.

[8]Green, A. E., and Lindsay, K. E., "Thermoelasticity," *Journal of Elasticity*, Vol. 2, No. 1, 1972, pp. 1–7.

[9]Chandrasekharaiah, D. S., "Thermoelasticity with Second Sound: A Review," *Applied Mechanics Reviews*, Vol. 39, No. 3, 1986, pp. 355–376.

[10]Joseph, D. D., and Preziosi, L., "Heat Waves," *Review of Modern Physics*, Vol. 61, No. 1, 1989, pp. 41–73.

[11]Joseph, D. D., and Preziosi, L., "Addendum to the Paper 'Heat Waves,'" *Review of Modern Physics*, Vol. 62, 1990, pp. 375–391.

[12]Nayfeh, A. H., "Propagation of Thermoelastic Distribution in Non-Fourier Solids," *AIAA Journal*, Vol. 15, 1977, pp. 957–960.

[13]Nayfeh, A. H., and Nemat-Nasser, S., "Thermoelastic Waves in Solid with Thermal Relaxation," *Acta Mechanics*, Vol. 12, 1971, pp. 53–69.

[14]Puri, P., "Plane Waves in Generalized Thermoelasticity," *International Journal of Engineering Science*, Vol. 11, 1973, pp. 735–744.

[15]Agarwal, V. K., "On Plane Waves in Generalized Thermoelasticity," *Acta Mechanics*, Vol. 31, 1979, pp. 185–198.

[16]Hosseini Tehrani, P., and Eslami, M. R., "Two-Dimensional Time Harmonic Dynamic Coupled Thermoelasticity Analysis by BEM Formulation," *Engineering Analysis with Boundary Elements*, Vol. 22, 1998, pp. 245–250.

[17]Prevost, J. H., and Tao, D., "Finite Element Analysis of Dynamic Coupled Thermoelasticity Problems with Relaxation Times," *Journal of Applied Mechanics*, Vol. 50, 1983, pp. 817–822.

[18]Tamma, K. K., and Railkar, S. B., "Evaluation of Thermally Induced Non-Fourier Stress Wave Disturbances via Specially Tailored Hybrid Trans-finite Formulations," *Computers and Structures*, Vol. 34, 1990, p. 5.

[19]Tamma, K. K., "Numerical Simulations for Hyperbolic Heat Conduction/Dynamic Problems Influenced by Non-Fourier/Fourier Effects," *Thermal Stresses IV*, edited by R. Hetnarski, Elsevier, Amsterdam, 1996.

[20]Tamma, K. K., and Namburu, R. R., "On Effective Finite Element Modeling/Analysis Approach for Dynamical Thermoelasticity due to Second Sound Effects," *Journal of Computational Mechanics*, Vol. 9, 1992, pp. 73–84.

[21]Chen, J., and Dargush, G. F., "BEM for Dynamic Proelastic and Thermoelastic Analysis," *Journal of Solids and Structures*, Vol. 32, No. 15, 1995, pp. 2257–2278.

[22]Chen, H. T., and Lin, H. J., "Study of Transient Coupled Thermoelastic Problems with Relaxation Times," *Journal of Applied Mechanics*, Vol. 62, March 1995, pp. 208–215.

[23]Eslami, M. R., and Hosseini Tehrani, P., "Propagation of Thermoelastic Waves in a Two-Dimensional Finite Domain by BEM," *Proceedings: Thermal Stresses*, Krakow Univ. of Technology, Krakow, Poland, 1999, pp. 551–560.

[24]Tosaka, N., "Boundary Integral Equation Formulations for Linear Coupled Thermoelasticity," *Proceedings of the 3rd Japan Symposium on BEM*, 1986, pp. 207–212.

[25]Durbin, F., "Numerical Inversion of Laplace Transforms: An Efficient Improvement to Dubner and Abate's Method," *Computer Journal*, Vol. 17, No. 4, 1974, pp. 371–376.

[26]Sternberg, E., and Chakravorty, J. G., "On Inertia Effects in a Transient Thermoelastic Problem," *Journal of Applied Mechanics*, Vol. 26, 1959, pp. 503–509.

G. A. Kardomateas
Associate Editor